

Phonon dispersions and vibrational properties of monolayer, bilayer, and trilayer graphene

Jia-An Yan, W. Y. Ruan, and M. Y. Chou

School of Physics, Georgia Institute of Technology, Atlanta, Georgia 30332-0430, U.S.A.

(Dated: October 29, 2018)

The phonon dispersions of monolayer and few-layer graphene (AB bilayer, ABA and ABC trilayers) are investigated using the density-functional perturbation theory (DFPT). Compared with the monolayer, the optical phonon E_{2g} mode at Γ splits into two and three doubly degenerate branches for bilayer and trilayer graphene, respectively, due to the weak interlayer coupling. These modes are of various symmetry and exhibit different sensitivity to either Raman or infrared (IR) measurements (or both). The splitting is found to be 5 cm^{-1} for bilayer and 2 to 5 cm^{-1} for trilayer graphene. The interlayer coupling is estimated to be about 2 cm^{-1} . We found that the highest optical modes at K move up by about 12 cm^{-1} for bilayer and 18 cm^{-1} for trilayer relative to monolayer graphene. The atomic displacements of these optical eigenmodes are analyzed.

PACS numbers:

I. INTRODUCTION

In recent years, monolayer and few-layer graphene have attracted great attention due to the unique properties observed experimentally.^{1,2,3} Many intriguing transport phenomena, such as ballistic transport at room temperature,^{4,5} the anomalous quantum Hall effect,^{6,7} and novel many-body couplings⁸ have been reported. In addition to being a physical system exhibiting novel properties, graphene and graphene layers have been proposed as promising candidates for future nanoelectronics. The epitaxial graphene grown on SiC is of particular interest due to the compatibility with current silicon technology.^{1,9}

Besides their unusual electronic structure,¹⁰ vibrational properties and phonon spectra are also of fundamental interest from which many physical properties (such as thermal conductivity and heat capacity) can be derived. Furthermore, phonons are crucial for studying the quasiparticle dynamics⁸ and electrical transport properties. Electrons excited by optical methods can be scattered into another states by electron-phonon coupling (EPC). It has been suggested that the scattering between electrons and the optical phonon modes greatly affects the high-field ballistic transport properties in carbon nanotubes.¹¹ In graphene and metallic single-wall nanotubes, the EPC strongly affects the phonon frequencies, giving rise to Kohn anomalies^{12,13} and possible soft modes or Peierls distortions.^{14,15}

Many experimental methods have been used to measure the phonon dispersions of graphite, such as inelastic neutron scattering (INS),¹⁶ electron-energy loss spectroscopy (EELS),¹⁷ high-resolution electron energy-loss spectroscopy (HREELS),¹⁸ and inelastic x-ray scattering (IXS).^{19,20} These measurements require large enough samples of crystalline quality and are limited to specific directions or phonon modes. More recently, Mohr et al.²⁰ have presented complete measurements of both the optical and the acoustic phonon modes along the directions Γ -K-M- Γ of graphite using IXS. The results in these mea-

surements are very close. In contrast to bulk graphite, Raman scattering has been widely used for probing the G-band in graphene layers that corresponds to the Γ phonons.^{21,22,23,24} Recently reported Raman spectra for graphene layers show that the intensity and position of the first-order G-band as well as the second order D-band (historically named the G' band) are modified with an increasing number of layers.^{21,22}

On the theoretical side, Grüneis et al.²⁵ presented the phonon dispersions of graphite using the 4th-nearest-neighbor force constant (4NNFC) approach. However, it has been argued that due to the Kohn anomaly at Γ and K, it is not possible to obtain the correct phonon dispersions near Γ and K from the force constant method.¹³ Dubay and Kresse¹⁴ performed density-functional theory (DFT) calculations of the phonon dispersions in graphite within the local density approximation (LDA). Their results are in good agreement with phonon-measurements by HREELS. Using the LDA and the generalized-gradient approximation (GGA), Wirtz and Rubio²⁶ calculated the phonon dispersions of graphite and obtained results close to the vast majority of the experimental data-points. At the GGA-PBE level, Mounet and Marzari²⁷ also presented a detailed calculation of the phonon dispersions of graphene and graphite.

With regard to graphene layers, it is unclear how the phonon properties are affected by the stacking order and the weak interlayer coupling. This effect is important for understanding the EPC in multilayer graphene as well as the interpretation of the Raman spectra. For example, the phonon dispersion around K is crucial for the correct interpretation of the Raman second order D peak. It has been shown that in few-layer graphene, the electronic dispersions near the Fermi level exhibit various features depending on the stacking order.¹⁰ In this work, the vibrational properties of one- and few-layer graphenes are calculated using density-functional perturbation theory (DFPT).²⁸ The monolayer, bilayer (AB stacking), and trilayer (ABA and ABC stackings) are considered in order to illustrate the effects of stacking order and inter-

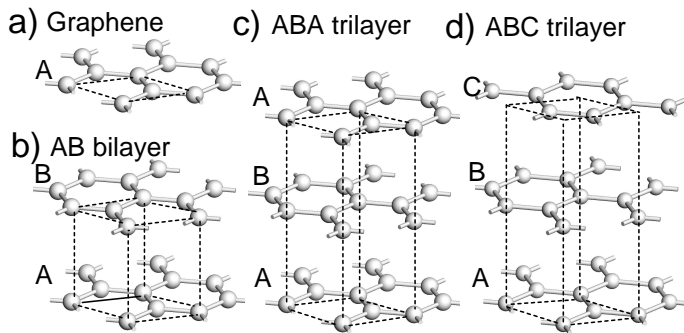


FIG. 1: Stacking structure for (a) monolayer, (b) AB bilayer, (c) ABA trilayer and (d) ABC trilayer graphene.

layer coupling. The van der Waals corrections in graphite have been shown to be important in order to correctly describe the long-range binding properties.^{29,30,31} However, previous theoretical calculations based on DFT with both LDA¹⁴ and GGA^{20,27} have indicated that rather reasonable vibrational properties of graphite can be obtained within DFT as compared with experiments. We find that the phonon dispersions for graphene and graphene layers exhibit somewhat different characteristics, especially at Γ and K. Detailed analysis of the phonon modes is also presented.

II. COMPUTATIONAL DETAILS

Density-functional calculations are performed using the ESPRESSO code³² with the LDA. Troullier-Martin (TM) norm-conserving pseudopotentials³³ generated from the valence configuration of $2s^22p^2$ for C are employed. The wavefunction and the charge density are expanded using energy cutoffs of 110 and 440 Ryd, respectively. Methfessel-Paxton smearing³⁴ with an energy width of 0.03 Ryd is adopted for the self-consistent calculations. The dynamical matrices are calculated based on DFPT within the linear response. For the integration over electronic states in the calculations, we use a $48 \times 48 \times 1$ uniform k-point mesh. A $6 \times 6 \times 1$ grid is used for the phonon calculation to obtain the dynamical matrices. We have carefully tested these parameters and the phonon frequencies are converged to be within 1 cm^{-1} .

Figure 1 shows the two-dimensional (2D) primitive cells for monolayer, bilayer (AB stacking), and trilayer graphene (ABA and ABC stacking). A large vacuum region of more than 10 \AA along the z direction is used to minimize the interactions between graphene layers in different supercells.

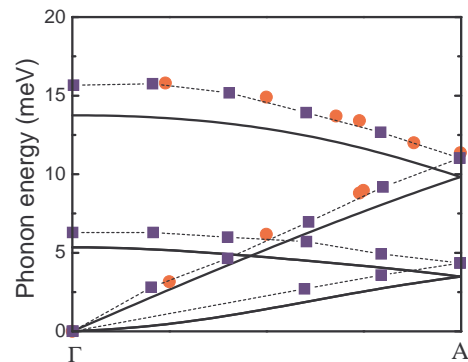


FIG. 2: (Color online) Phonon dispersions of graphite along the Γ -A direction. Solid lines are present computational results. Circles are IXS data from Ref. 20, and squares are neutron scattering data from Ref. 16. The dotted lines are smooth curves through the measured points.

III. RESULTS AND DISCUSSIONS

The optimized LDA lattice constant in the graphene plane is 2.45 \AA , in good agreement with the previous calculated result,¹⁰ which is also close to the experimental value of 2.46 \AA for graphite.³⁵ For the bilayer and trilayer systems, the lattice constant in the plane remains almost the same as in graphene. The optimized interlayer spacing is 3.33 \AA , slightly smaller than the experimental value of 3.35 \AA in bulk graphite.³⁵ In comparison, we obtained a theoretical value of 3.32 \AA for graphite, which is close to previous LDA results.³⁶ The interlayer binding energy (defined as the total energy difference between the coupled and uncoupled graphene layers) of bulk graphite is calculated to be 25.2 meV/atom , while this energy falls to 12.3 meV/atom for an AB bilayer. For the ABA and ABC trilayer, the interlayer binding energies are both 16.5 meV/atom . Our result of graphite is comparable to previous calculations using a combined density-functional and intermolecular perturbation theory approach.³¹ To validate the DFPT phonon calculations, we also calculated the low energy phonon dispersions in bulk graphite along the Γ -A direction (perpendicular to the layers), as shown in Fig. 2. Except for a small frequency shift, our LDA dispersions agree with experimental data rather well. Therefore, we believe our calculations yield reliable descriptions of the phonon properties in graphite and graphene layers. This agreement between LDA and experimental results indicate an error cancellation for energy variations near the equilibrium layer separation, even though the state-of-the-art local or semilocal exchange-correlation functionals are not able to properly describe the long-range interlayer interactions dominated by van der Waals dispersion forces (see Refs. [37] and [38] for details).

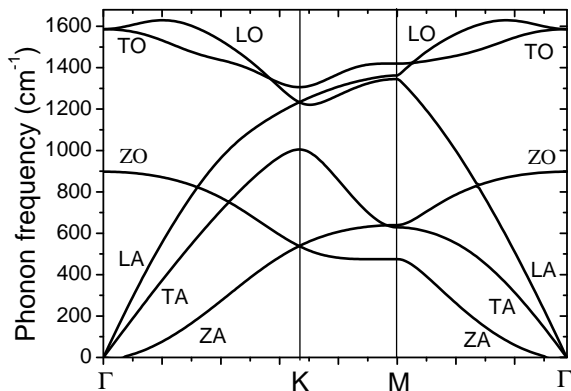


FIG. 3: Phonon dispersions for monolayer graphene.

A. Phonon Properties of Graphene

Figure 3 shows the phonon dispersions for monolayer graphene calculated at the theoretical lattice constant, which will be compared with multilayer results in the next section. In contrast to the linear dispersion near the Γ point for the in-plane TA and LA modes, the out-of-plane ZA mode shows a q^2 dispersion, which is a characteristic feature of the phonon dispersions in layered crystals as observed experimentally.^{27,39,40} The same feature also appears in bilayer and trilayer phonon dispersions, as will be discussed in Section III B.

The calculated frequency (1586 cm^{-1}) of the degenerate LO and TO modes at Γ is slightly smaller than the previous value of 1595 cm^{-1} obtained by Dubay *et al.*,¹⁴ but is in excellent agreement with the experimental result of 1587 cm^{-1} by inelastic x-ray scattering measurements.¹⁹ At the Brillouin zone corner K, the phonon energy of the symmetric TO A'_1 mode (1306 cm^{-1}) is close to the frequency (1326 cm^{-1}) calculated by Wirtz *et al.*²⁶ Our result is also consistent with the estimate by Yao *et al.*⁴¹ from their high-voltage transport measurements for graphite. They suggested that scattering by phonons with an energy of about 1300 cm^{-1} gives rise to the dramatic conductance drop at a high bias. In general, our calculated phonon dispersions for monolayer graphene are comparable with those obtained in previous calculations^{14,26} and agree very well with experimental results.^{19,41}

A previous study by Piscanec *et al.*¹³ showed that the degenerate E_{2g} modes at Γ and the highest TO mode at K have a strong EPC, leading to Kohn anomalies in the phonon dispersions. A detailed analysis of the origin of the strong EPC for these modes is presented below.

For a specific phonon mode ν with wave vector q , the displacement of atom j ($j=\alpha,\beta$) in unit cell m will oscillate according to the following expression in the classical picture:

$$\vec{u}_{q\nu}^{mj} = \sum_{s=x,y,z} \hat{e}_s \text{Re}\{e_{q\nu,s}^j e^{i(\vec{q}\cdot\vec{R}_m - \omega_{q\nu}t)}\}$$

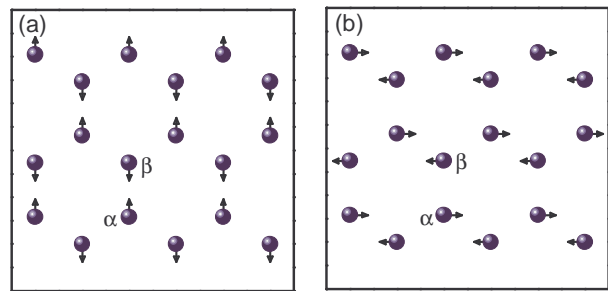


FIG. 4: (Color online) Pattern of atomic displacements for the TO/LO modes at Γ in monolayer graphene.

$$= \sum_{s=x,y,z} \hat{e}_s |e_{q\nu,s}^j| \cos(\vec{q}\cdot\vec{R}_m - \omega_{q\nu}t + \phi_{q\nu,s}^j), \quad (1)$$

where \vec{R}_m is the lattice vector for unit cell m , $\phi_{q\nu,s}^j$ denotes the phase factor of the complex eigenvector $e_{q\nu,s}^j$, and $\omega_{q\nu}$ is the phonon frequency.

For the degenerate TO/LO phonon modes at Γ , Figs. 4(a) and (b) schematically show the atomic displacements associated with the two eigenmodes. Clearly, two neighboring atoms vibrate opposite to one another. This gives rise to a large bond distortion and couples to electronic states near the Dirac point (which can be projected into two states localized at atom α and β , respectively) through an intravalley scattering (with phonon $q\approx 0$). Therefore, a strong EPC is expected, which has also been demonstrated by the effective mass theory⁴² as well as the tight-binding model.⁴³

In contrast, for the highest TO A'_1 mode at K the classical displacements of neighboring atoms α and β follow the pattern

$$\vec{u}^\alpha = u_0 [\hat{e}_x \cos(\frac{\pi}{2} - \omega t) - \hat{e}_y \sin(\frac{\pi}{2} - \omega t)], \quad (2)$$

$$\vec{u}^\beta = u_0 [\hat{e}_x \cos(\frac{\pi}{2} - \omega t) + \hat{e}_y \sin(\frac{\pi}{2} - \omega t)] \quad (3)$$

and atoms α and β move circularly. In particular, one moves counterclockwise, while the other clockwise, as shown in Fig. 5. Accordingly, each atom approaches its three nearest neighbors successively during one period. Fig. 5 shows three snapshots of the atomic displacements in one period.

Since the degenerate electronic states at the Dirac point can be projected into two states localized at atom α and β , respectively, the above mode of ionic vibration facilitates the transition of an electron from atoms α to β or vice versa, resulting in the electronic intervalley scattering via a phonon with momentum \vec{K} . Therefore, a strong EPC is expected for this mode compared with other modes at K.⁴⁴ Based on the detailed analyses of these modes, we anticipate a distinct electron-phonon interactions for these modes in few-layer graphene. The results will be presented elsewhere.

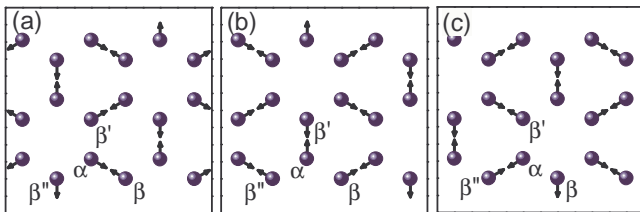


FIG. 5: (Color online) Three snapshots of atomic displacements for the highest TO mode at K in monolayer graphene, where atom α approaches its three nearest neighbors β (a), β' (b), and β'' (c) successively.

B. Phonon Dispersions for Graphene Layers

In this section, we focus on the optical phonon modes in multilayer graphene. The phonon dispersions for bilayer and trilayer are shown in Fig. 6 (a). The detailed dispersions for the high optical branches near Γ and K are enlarged in Figs. 6(b) and (c), respectively. The optical phonon frequencies are also listed in Table I.

Compared with the monolayer result, several distinct features can be identified for graphene multilayers. First, there is one (two) additional low-frequency mode with energy of about 90 cm^{-1} at Γ in bilayer (trilayer) graphene. These modes arise from interlayer movement (so-called ‘layer breathing’ modes). Second, at Γ the doubly degenerate E_{2g} branch in the monolayer evolves into two (three) doubly degenerate branches for bilayer (trilayer) graphene, as shown in Fig. 6(b). These small splittings are due to the weak interlayer coupling: about 5 cm^{-1} for bilayer and no more than 5 cm^{-1} for trilayer (see Table I). Moving away from Γ , each of these degenerate branches breaks into two different modes. Recent experiments show that the Raman G-peak intensity enhances almost linearly with respect to the layer number (up to four layers).^{21,23} This phenomenon could be ascribed to the increased number of optical phonon modes at Γ within a small energy window for multilayer graphene.

The stackings of graphene layers have various point group symmetry for the Γ phonons. The monolayer graphene possesses the D_{6h} symmetry (Schönflies notation). It reduces to D_{3d} for the AB bilayer and ABC trilayer, and D_{3h} for the ABA trilayer. Correspondingly, their high optical zone-center modes are of different mode symmetry: E_{2g} mode in graphene evolves into E_g and E_u for the AB bilayer, $2E'+E''$ for the ABA trilayer, and $2E_g+E_u$ for the ABC trilayer. The E_g and E'' modes are Raman active, E_u is IR active, while the E' modes are both Raman and IR active. Therefore, a complete picture of the zone-center modes can be obtained from a combination of Raman and IR measurements. These mode splittings provide significant information about the layer number and the stacking geometry.

In Figs. 7-9, we show the schematic atomic displacements of these optical eigenmodes at Γ for the AB bilayer, ABA trilayer, and ABC trilayer, respectively. These

high-frequency phonons are derived from the superpositions of intralayer optical modes in each graphene plane. For the modes in the bilayer as shown in Fig. 7, the two atoms on top of each other in two adjacent layers vibrate either in the opposite direction (E_g mode, 1587 cm^{-1}) or in the same direction (E_u mode, 1592 cm^{-1}). Similar atomic displacements can also be seen in ABA and ABC trilayers, as shown in Figs. 8 and 9. In other words, the original intralayer modes couple to each other via interlayer interactions, giving rise to a small splitting in the final frequencies. The upper and lower modes in the bilayer correspond to the ‘in-phase’ and ‘out-of-phase’ superpositions of the two intralayer modes, respectively, similar to the E_{1u} and E_{2g} modes in bulk graphite.

This splitting of the phonon frequencies at Γ can be illustrated using a simple model. Using the original intralayer optical modes as the basis and assuming the interaction strength between adjacent layers is ϵ , the reduced Hamiltonian for the bilayer and trilayer can be expressed as:

$$H_2 = E_0 I + \begin{pmatrix} 0 & \epsilon \\ \epsilon & 0 \end{pmatrix} = \begin{pmatrix} E_0 & \epsilon \\ \epsilon & E_0 \end{pmatrix} \quad (4)$$

and

$$H_3 = \begin{pmatrix} E_0 & \epsilon & 0 \\ \epsilon & E_0 + \delta & \epsilon \\ 0 & \epsilon & E_0 \end{pmatrix}, \quad (5)$$

respectively. Here, E_0 is the energy of the intralayer mode, and only the first nearest-neighbor layer-layer interaction is considered. For the trilayer, a small variant of δ is introduced in Eq. (5) to account for the change of the on-site energy in the middle layer due to the new geometry. (This is similar to the on-site energy variation due to environmental changes in electronic tight-binding models.^{45,46}) Solving the secular equation $\det(H - \lambda I) = 0$, one obtains the eigenvalues and eigenvectors.

For the bilayer, the eigenvalues are $\lambda_{1,2} = E_0 \pm \epsilon$. From Fig. 7, the E_0 and ϵ can be determined: $E_0 = 1589.5$ and $|\epsilon| = 2.5 \text{ cm}^{-1}$. E_0 shows a small shift compared with the value for a single-layer graphene (1586 cm^{-1}) as a result of the environmental change mentioned above. With $\epsilon > 0$, the corresponding eigenvectors are $\phi_{1,2} = (1, \pm 1)^T$. This is consistent with the displacements we obtained in Fig. 7. The lower frequency corresponds to the out-of-phase superposition of the two intralayer modes (with respect to the motion of the two atoms on top of each other in two adjacent layers), while the higher one corresponds to the in-phase superposition. In both cases, the two intralayer modes have equal amplitudes.

For the trilayer, the eigenvalues are $\lambda_1 = E_0$, $\lambda_{2,3} = E_0 + (\delta \pm \sqrt{\delta^2 + 8\epsilon^2})/2$, with corresponding eigenvectors $\phi_1 = (1, 0, -1)^T$, $\phi_{2,3} = (\epsilon, (\delta \pm \sqrt{\delta^2 + 8\epsilon^2})/2, \epsilon)^T$. For the latter two eigenvectors, the ratio of the mode amplitudes in each layer is $a_1 : a_2 : a_3 = \epsilon : (\delta \pm \sqrt{\delta^2 + 8\epsilon^2})/2 : \epsilon$. Using the frequencies for the ABA trilayer as shown in Fig. 8, we obtain $\delta \approx 3 \text{ cm}^{-1}$ and $\epsilon \approx 2.2 \text{ cm}^{-1}$, and the

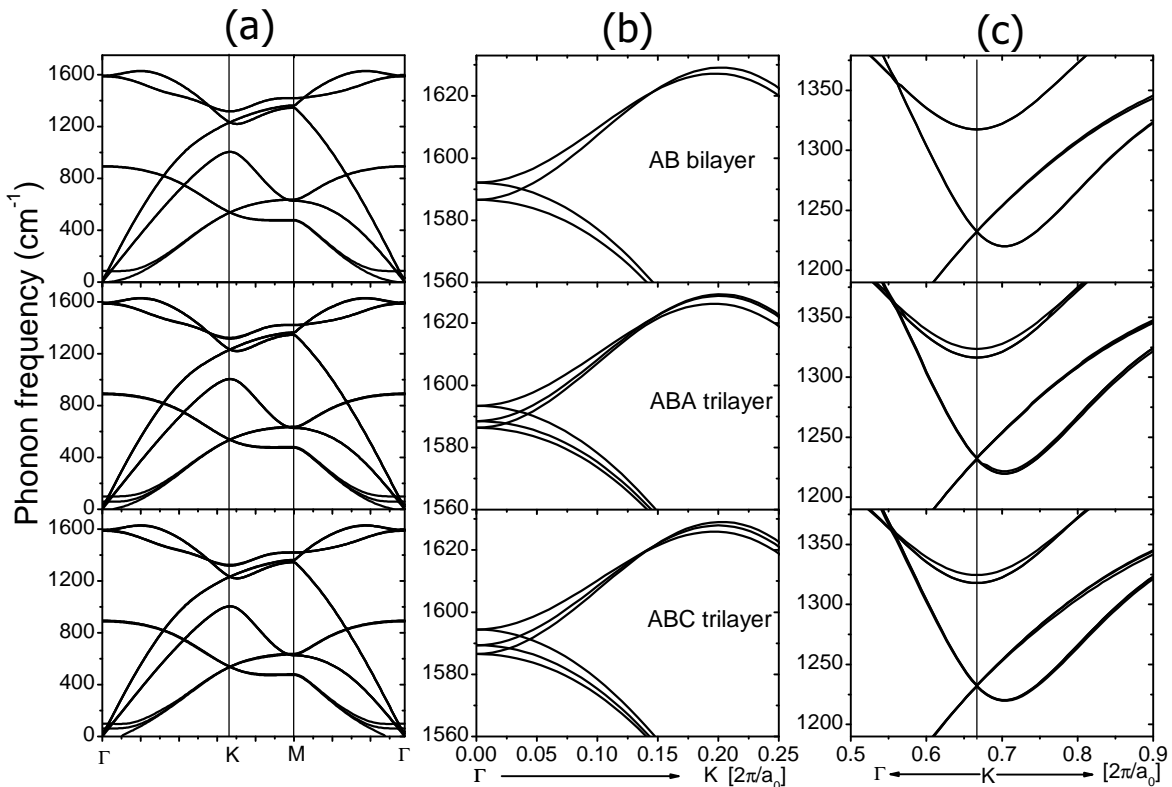


FIG. 6: Phonon dispersions for graphene multilayers. From top to bottom: AB bilayer, ABA trilayer, and ABC trilayer. Column (a): full phonon spectra; column (b): optical phonon dispersions near Γ ; column (c): optical phonon dispersions near K.

TABLE I: High optical phonon frequencies ω (in cm^{-1}) at Γ and K for monolayer, bilayer, trilayer graphene, and bulk graphite. The phonon frequencies at Γ and K from recent DFT calculations (with LDA and GGA) as well as experimental measurements are listed for comparison. The point group symmetry at Γ (K) for the monolayer, AB bilayer, ABA trilayer, ABC trilayer, and graphite is D_{6h} (D_{3h}), D_{3d} (C_{3v}), D_{3h} (C_{3h}), D_{3d} (C_{3v}), and D_{6h} (D_{3h}), respectively. In parentheses are the mode symmetries.

	Graphene	AB	ABA	ABC	Graphite	Graphite exp.
Γ	1586 (E_{2g}) 1595 ^a , 1597 ^{b,c} 1569 ^d , 1581 ^e	1587 (E_g) 1592 (E_u)	1586 (E') 1588 (E'') 1593 (E')	1586 (E_g) 1589 (E_u) 1594 (E_g)	1586 (E_{2g}) 1595 (E_{1u})	1582 ^f , 1581 ^h 1588 ^g
K	1306 (A'_1) 1371 ^a , 1326 ^c 1289 ^d , 1300 ^e 1265 ^h	1318 (E)	1316 (E'_1, E''_1) 1324 (E'_2)	1318 (E) 1325 (A_1)	1322 (E)	

^aLDA, soft projector augmented wave (PAW), Ref. [14].

^bLDA, Hard PAW, Ref. [14].

^cLDA, TM potentials, Ref. [26].

^dGGA, TM potentials, Ref. [26].

^eGGA, Ref. [19].

^fExpt. $\omega(E_{2g})$, Refs.[47,48,49].

^gExpt. $\omega(E_{1u})$, Ref. [47] and [50].

^hInelastic X-ray data of Ref. [19] and [20].

mode amplitude ratios of 2.2:5.0:2.2 and 2.2:(-2.0):2.2 for these two modes, respectively. This result agrees with the displacements from the direct first-principles calculations shown in Fig. 8. Similar results can be obtained for the ABC trilayer. Based on these numerical results,

one can easily estimate the optical phonon frequencies for more graphene layers using an interlayer interaction of 2-3 cm^{-1} and the values of E_0 and δ obtained above.

The highest optical phonon branch at K becomes doubly degenerate at 1318 cm^{-1} in the bilayer system (see

Table I), nearly 12 cm^{-1} higher than that in graphene. The degeneracy is imposed by the symmetry of the bilayer. The two degenerate modes correspond to two intralayer modes within individual layers with little coupling between them. In contrast, the optical phonons in the ABA split into three modes, with two of them being almost degenerate, while the degeneracy is imposed by symmetry in the ABC trilayer. For the ABA and ABC trilayers, the highest phonon (singlet) frequencies are 1324 and 1325 cm^{-1} , respectively. This result is consistent with the Raman observation that the second-order D mode at about 2700 cm^{-1} increases with an increasing layer number.⁵¹ The second-order D mode in the Raman spectrum of graphene and graphene layers, which is double of the highest optical phonon frequency at K, can be well illustrated using a double-resonant model.⁵¹

Figure 10 shows the schematic atomic displacements of the three eigenmodes at K for the ABA trilayer. Each eigenmode comprises a superposition of the intralayer A_1' modes from each layer. As shown in Fig. 10, the two almost degenerate low-frequency modes (about 1316 cm^{-1}) correspond to the combinations of the modes from the top and bottom A layers, while the high branch is an intralayer mode from the middle B layer almost exclusively.

The splitting in frequencies at K can be analyzed in a similar way as before. In contrast to the Γ phonons, the coupling between adjacent intralayer modes is zero due to the mode symmetry, and there might only be a small interaction between the top and the bottom layers. In this case, the Hamiltonian can be expressed as:

$$H = \begin{pmatrix} E'_0 & 0 & \eta \\ 0 & E'_0 + \delta' & 0 \\ \eta & 0 & E'_0 \end{pmatrix}, \quad (6)$$

with η the small interaction between second nearest-neighbor layers. The eigenvalues are $\lambda = E'_0 \pm \eta$, and $E'_0 + \delta'$. According to the frequencies as shown in Fig. 10, we obtain $\delta' = 7.2 \text{ cm}^{-1}$ and $|\eta| = 0.2 \text{ cm}^{-1}$. The amplitudes are $a_1 : a_2 : a_3 = \pm 1 : 0 : 1$ for $\lambda = E'_0 \pm \eta$, and $0 : 1 : 0$ for $\lambda = E'_0 + \delta'$. This is consistent with the atomic displacements illustrated in Fig. 10 with $\eta < 0$. Note that the small interactions between second nearest-neighbor layers have induced a small splitting of the two low-frequency modes.

In the case of ABC stacking, the interlayer coupling matrix elements are identically zero. Therefore, the three eigenmodes at K are localized on each of the three layers, respectively. Due to the higher on-site energy in the middle layer, one state will be higher than the other two modes, with the lower two modes doubly degenerate due to the symmetry.

IV. SUMMARY

In summary, we have studied the phonon dispersions and vibrational properties for monolayer, bilayer, and tri-

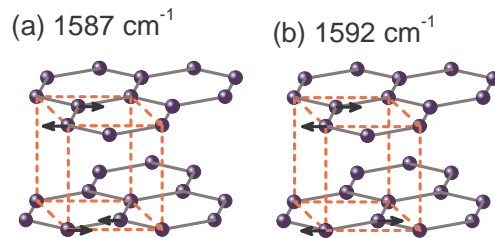


FIG. 7: (Color online) Atomic displacements of the two split optical branches (a) 1587 , and (b) 1592 cm^{-1} at Γ for the AB bilayer. Only one mode for each degenerate pair is shown.

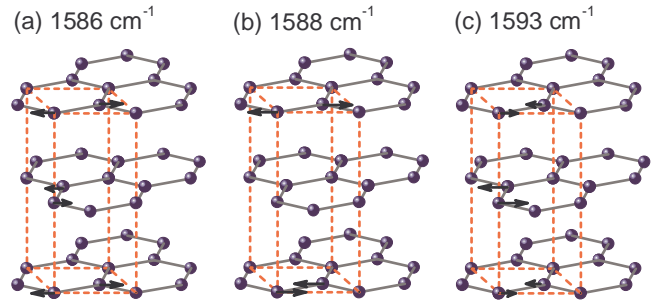


FIG. 8: (Color online) Atomic displacements of the three split optical branches (a) 1586 , (b) 1588 , and (c) 1593 cm^{-1} at Γ for the ABA trilayer. The length of the arrow represents the amplitude of the eigenvector. Only one mode for each degenerate pair is shown.

layer graphene using the density-functional perturbation theory. Due to the weak coupling between layers, the highest optical phonon branch at Γ in graphene splits into two (three) doubly degenerate branches with small yet unnegligible splittings for bilayer (trilayer) graphene. The splitting is about 5 cm^{-1} for the bilayer. In trilayer ABA and ABC graphene, these splittings are about 2 cm^{-1} and 5 cm^{-1} , respectively, which are not equally spaced. These modes are of various mode symmetry and exhibit different sensitivity to either Raman or IR measurements and therefore a combination of Raman and IR

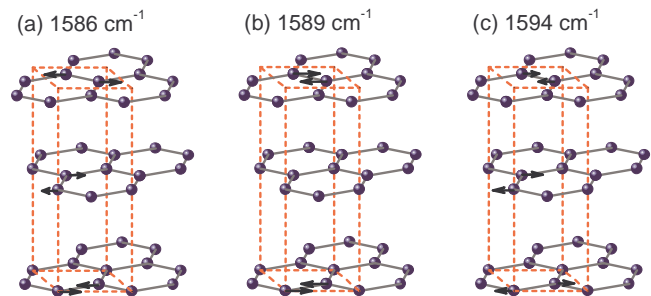


FIG. 9: (Color online) Atomic displacements of the three split optical branches (a) 1586 , (b) 1589 , and (c) 1594 cm^{-1} at Γ for the ABC trilayer. The length of the arrow represents the amplitude of the eigenvector. Only one mode for each degenerate pair is shown.

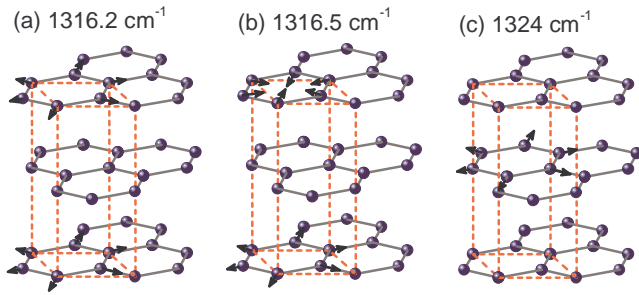


FIG. 10: (Color online) Atomic displacements of the three optical phonon modes (a) 1316.2, (b) 1316.5, and (c) 1324 cm^{-1} at K for the ABA trilayer. The length of the arrow represents the amplitude of the eigenvector. Only one mode for each degenerate pair is shown.

measurements of the zone-center optical modes should give a clear identification of the layer number as well as the stacking geometry.

A simple interaction model is applied to illustrate the frequency splitting and the characteristics of the eigenmodes at Γ . The interlayer coupling strength is identified as about 2 cm^{-1} . In the trilayer system, a shift of about 3 cm^{-1} in the on-site energy in the middle layer is determined.

The frequency of the highest optical phonon mode at K in bilayer (trilayer) graphene is about 12 (18) cm^{-1} higher than that in monolayer graphene. For trilayer graphene, the $\text{K-A}_1'$ mode splits into three branches in the ABA trilayer, with the two lower modes nearly doubly degenerate. It is found that the on-site energy variations for the middle layer in ABA and ABC are about 7-8 cm^{-1} , higher than that of Γ phonons. Due to the symmetry, the interlayer coupling between adjacent layers for these intralayer modes is zero.

Acknowledgments

We acknowledge helpful discussions with M. Wierzbowska, S. Piscanec, and A. C. Ferrari. We thank M. Mohr for providing the experimental data of bulk graphite. This work is supported by the Department of Energy (Grant No. DE-FG02-97ER45632) and by the National Science Foundation (Grants No. DMR-02-05328). The computation used resources of the National Energy Research Scientific Computing Center (NERSC), which is supported by the U.S. Department of Energy (Grant No. DE-AC03-76SF00098), and San Diego Supercomputer Center (SDSC) at UCSD.

- ¹ W. A. de Heer, C. Berger, X. Wu, P. N. First, E. H. Conrad, X. Li, T. Li, M. Sprinkle, J. Hass, M. L. Sadowski, M. Potemski, G. Martinez, *Solid State Commun.* **143**, 92 (2007)..
- ² A. K. Geim, and K. S. Novoselov, *Nature Materials* **6**, 183 (2007).
- ³ For a recent review, see M. I. Katsnelson, *Mater. Today*, **10**, 20 (2007), and references therein.
- ⁴ C. Berger, Z. M. Song, T. B. Li, X. B. Li, A. Y. Ogbazghi, R. Feng, Z. T. Dai, A. N. Marchenkov, E. H. Conrad, P. N. First, and W. A. de Heer, *J. Phys. Chem. B* **108**, 19912 (2004).
- ⁵ C. Berger, Z. Song, T. Li, X. Li, A. Y. Ogbazghi, R. Feng, Z. Dai, A. N. Marchenkov, E. H. Conrad, P. N. First, W. A. de Heer, *Science* **312**, 1191 (2006).
- ⁶ K. S. Novoselov, A. K. Geim, S. V. Morozov, D. Jiang, M. I. Katsnelson, I. V. Grigorieva, S. V. Dubonos, A. A. Firsov, *Nature* **438**, 197 (2005).
- ⁷ Y. Zhang, Y. W. Tan, H. L. Stormer, and P. Kim, *Nature* **438**, 201 (2005).
- ⁸ A. Bostwick, T. Ohta, T. Seyller, K. Horn and Eli Rotenberg, *Nature Physics* **3**, 36 (2007).
- ⁹ J. Hass, R. Feng, J. E. Millan-Otoya, X. Li, M. Sprinkle, P. N. First, C. Berger, W. A. de Heer, and E. H. Conrad, *Physical Rev. B* **75**, 214109 (2007).
- ¹⁰ S. Latil, and L. Henrard, *Phys. Rev. Lett.* **97**, 036803 (2006).
- ¹¹ M. Lazzeri, S. Piscanec, F. Mauri, A. C. Ferrari, and J. Robertson, *Phys. Rev. Lett.* **95**, 236802 (2005).
- ¹² W. Kohn, *Phys. Rev. Lett.* **2**, 393 (1959).
- ¹³ S. Piscanec, M. Lazzeri, F. Mauri, A. C. Ferrari, and J. Robertson, *Phys. Rev. Lett.* **93**, 185503 (2004).
- ¹⁴ O. Dubay, G. Kresse, *Phys. Rev. B* **67**, 035401 (2003).
- ¹⁵ S. Piscanec, M. Lazzeri, J. Robertson, A. C. Ferrari, and F. Mauri, *Phys. Rev. B* **75**, 035427 (2007).
- ¹⁶ R. Nicklow, N. Wakabayashi, and H. G. Smith, *Phys. Rev. B* **5**, 4951 (1972).
- ¹⁷ C. Oshima, T. Aizawa, R. Souda, Y. Ishizawa, and Y. Sumiyoshi, *Solid State Commun.* **65**, 1601 (1988).
- ¹⁸ S. Siebentritt, R. Pues, K.-H. Rieder, and A. M. Shikin, *Phys. Rev. B* **55**, 7927 (1997).
- ¹⁹ J. Maultzsch, S. Reich, C. Thomsen, H. Requardt, P. Ordejón, *Phys. Rev. Lett.* **92**, 075501 (2004).
- ²⁰ M. Mohr, J. Maultzsch, E. Dobardžić, S. Reich, I. Milošević, M. Damnjanović, A. Bosak, M. Krisch, and C. Thomsen, *Phys. Rev. B* **76**, 035439 (2007).
- ²¹ D. Graf, F. Molitor, K. Ensslin, C. Stampfer, A. Jungen, and C. Hierold, and L. Wirtz, *Nano Lett.* **7**, 238 (2007).
- ²² A. C. Ferrari, J. C. Meyer, V. Scardaci, C. Casiraghi, M. Lazzeri, F. Mauri, S. Piscanec, D. Jiang, K. S. Novoselov, S. Roth, and A. K. Geim, *Phys. Rev. Lett.* **97**, 187401 (2006).
- ²³ A. Gupta, G. Chen, P. Joshi, S. Tadigadapa, and P.C. Eklund, *Nano Lett.* **6**, 2667 (2006).
- ²⁴ J. Yan, Y. Zhang, P. Kim, and A. Pinczuk, *Phys. Rev. Lett.* **98**, 166802 (2007).
- ²⁵ A. Grüneis, R. Saito, T. Kimura, L. G. Cancado, M. A. Pimenta, A. Jorio, A. G. Souza Filho, G. Dresselhaus, M. S. Dresselhaus, *Phys. Rev. B* **65**, 155405 (2002).
- ²⁶ L. Wirtz, A. Rubio, *Solid State Comm.* **131**, 141(2004).
- ²⁷ N. Mounet and N. Marzari, *Phys. Rev. B* **71**, 205214 (2005).

- ²⁸ S. Baroni, S. de Gironcoli, and A. Dal Corso, *Rev. Mod. Phys.* **73**, 515 (2001).
- ²⁹ L. A. Girifalco and M. Hodak, *Phys. Rev. B* **65**, 125404 (2002).
- ³⁰ S. D. Chakarova-Käck, E. Schröder, B. I. Lundqvist, and D. C. Langreth, *Phys. Rev. Lett.* **96**, 146107 (2006).
- ³¹ Y. J. Dappe, M. A. Basanta, F. Flores, and J. Ortega, *Phys. Rev. B* **74**, 205434 (2006).
- ³² S. Baroni, A. Dal Corso, S. de Gironcoli, P. Giannozzi, C. Cavazzoni, G. Ballabio, S. Scandolo, G. Chiarotti, P. Focher, A. Pasquarello, K. Laasonen, A. Trave, R. Car, N. Marzari, A. Kokalj, <http://www.pwscf.org/>
- ³³ N. Troullier and J. L. Martins, *Phys. Rev. B* **43**, 1993 (1991).
- ³⁴ M. Methfessel and A. T. Paxton, *Phys. Rev. B* **40**, 3616 (1989).
- ³⁵ R. W. G. Wyckoff, *Crystal Structure*, Vol. 1 (Interscience, New York, 1963).
- ³⁶ N. Ooi, A. Rairkar, J. B. Adams, *Carbon* **44**, 231 (2006).
- ³⁷ W. Kohn, Y. Meir, and D. E. Makarov, *Phys. Rev. Lett.* **80**, 4153 (1998).
- ³⁸ H. Rydberg, M. Dion, N. Jacobson, E. Schroder, P. Hyldgaard, S. I. Simak, D. C. Langreth, and B. I. Lundqvist, *Phys. Rev. Lett.* **91**, 126402 (2003).
- ³⁹ H. Zabel, *J. Phys.: Condens. Matter* **13**, 7679 (2001).
- ⁴⁰ I. M. Lifshitz, *Zh. Eksp. Teor. Fiz.* **22**, 475 (1952).
- ⁴¹ Z. Yao, C. L. Kane, and C. Dekker, *Phys. Rev. Lett.* **84**, 2941 (2000).
- ⁴² T. Ando, *J. Phys. Soc. Jpn.* **75**, 124701 (2006).
- ⁴³ J. Jiang, R. Saito, A. Grüneis, G. Dresselhaus, and M. S. Dresselhaus, *Chem. Phys. Lett.* **392**, 383 (2006).
- ⁴⁴ M. Lazzeri and F. Mauri, *Phys. Rev. Lett.* **97**, 266407 (2006).
- ⁴⁵ D. J. Chadi, in: V. Vitek and D. J. Srolovitz (Eds), *Atomistic Simulations of Materials: Beyond Pair Potentials* (Plenum Press, New York and London, 1989) p.309.
- ⁴⁶ J. L. Mercer, and M. Y. Chou, *Phys. Rev. B* **49**, R8506 (1994).
- ⁴⁷ R. J. Nemanich, S. A. Solin, *Phys. Rev. B* **20**, 392 (1979).
- ⁴⁸ F. Touinstra, J. L. Koenig, *J. Chem. Phys.* **53**, 1126 (1970).
- ⁴⁹ L. J. Brillson, E. Burstein, A. A. Maradudin, T. Stark, in: D. L. Carter, R. T. Bate (Eds.), *The Physics of Semimetals and Narrow Gap Semiconductors* (Pergamon, Oxford, 1997), p. 187.
- ⁵⁰ R. A. Friedel, G. C. Carlson, *J. Phys. C* **75**, 1149 (1971).
- ⁵¹ A. C. Ferrari, *Solid State Commun.* **143**, 47 (2007).